The utility of three-dimensional dynamic contrast-enhanced magnetic resonance imaging in delineating vessel-rich regions: a case report of an aneurysmal bone cyst of the mandible

Abstract

Aneurysmal bone cysts (ABCs) are classified as bone-related lesions based on the 2005 World Health Organization histological classification of odontogenic tumors. Most ABCs are diagnosed using a combination of conventional radiography, computed tomography, magnetic resonance imaging (MRI), and digital subtraction angiography. ABCs should be differentiated from true cysts or other pseudocysts because their treatment is different. Additionally, unlike other cysts, ABCs pose a hemorrhagic risk in surgery; thus, preoperative evaluation of intralesional blood flow is required. Here we report a case of a mandibular ABC in a 39-year-old woman and focus on the cyst's magnetic resonance (MR) features using dynamic contrast-enhanced MRI (DCE-MRI). On DCE-MRI, the lesion was divided into two areas according to the enhancement pattern: the blood-pooling and blood-flow areas. The series of DCE-MR images of the blood-pooling area showed marked enhancement of the margin, but no enhancement in the inner part of the cavity. Additionally, the time-signal intensity curve (TIC) demonstrated no change in the signal intensity (SI) until approximately 15 min after gadolinium-diethylenetriamine penta-acetic acid (Gd-DTPA) administration. In contrast, the series of DCE-MR images of the blood-flow area exhibited marked enhancement in the cyst cavity in the early phase. The TIC showed a rapid increase in SI in the early phase, followed by a rapid decrease until 150 s, and finally a gradual decrease until approximately 15 min after Gd-DTPA administration. Thus, in the current case, preoperative DCE-MRI clearly delineated the vessel-rich area within the lesion.

Key Words: aneurysmal bone cyst, dynamic contrast-enhanced MRI, MRI

Introduction

Aneurysmal bone cysts (ABCs) are classified as bone-related lesions according to the 2005 World Health Organization (WHO) histological classification of odontogenic tumors [1]. ABCs are relatively rare, nonneoplastic expansile lesions of the bone that are commonly found in the long bones and spine [2, 3], and seldom involve the jaws [4, 5]. Bleeding may occur during biopsy or surgery for ABCs because they are aneurysms with numerous pools of blood [6, 7]. Thus, before ABC treatment or biopsy is initiated, noninvasive methods should be used for lesion diagnosis [8]. Most ABCs are diagnosed using conventional radiography, computed tomography (CT), magnetic resonance imaging (MRI), and digital subtraction angiography (DSA). However, some cases may be difficult to diagnose even if examined by contrast-enhanced CT or MRI. Conversely, dynamic contrast-enhanced MRI (DCE-MRI) can provide hemodynamic information and measure lesion vascularity. Thus, we report a case of ABC in the mandible with a focus on DCE-MRI to evaluate blood flow.

Case report

The radiographic, CT, and MRI findings of the present case have already been reported in the *Japanese Journal of Oral Diagnosis/Oral Medicine* [9], but a diagnosis of ABC was not made at that time. Subsequently, we reexamined the imaging features, in addition to the DCE-MRI findings, and obtained information for differential diagnosis of ABC.

A 39-year-old woman was referred to our hospital for examination of radiolucency of the left mandible, which had been detected in a general dental clinic. She had experienced tenderness at the left mandible for 2 years.

On clinical examination, a bone-like swelling at the left body of the mandible was observed. Intraoral examination revealed percussion pain at the left premolar and molar regions. Her general medical and family histories were noncontributory with no history of facial trauma.

Imaging studies to evaluate this lesion included plain X-rays (X-Ps), CT, MRI, and DSA.

A panoramic radiograph revealed a large expansile, multilocular lesion with a thin bony rim in the left mandible, which was enlarged from the left first premolar to the mandibular ramus. CT images revealed buccolingual bony expansion and cortical thinning. The lesion had a low attenuation value between 20 and 30 Hounsfield units, which is consistent with a tissue composed of liquid. These findings have already been reported in the *Japanese Journal of Oral Diagnosis/Oral Medicine* [9].

MRI was performed on a 1.5-T unit (Magnetom Vision; Siemens, Erlangen, Germany) with a head-neck coil. T1-weighted images (T1WIs) and T2-weighted axial images were acquired using a turbo spin-echo sequence ((repetition time (TR) = 620 ms; echo time (TE) = 15 ms) and (TR = 2500 ms; TE = 105 ms), respectively).

DCE-MR images were acquired using three-dimensional (3-D) fast imaging with a steady-state precession sequence using the following parameters: TR, 5 ms; TE, 2 ms; flip angle, 25°; 16 partitions for a 48-mm slab resulting in an effective thickness of 3 mm; and a 250 × 188-mm rectangular field of view and 256 × 192 matrix (resulting in a 0.98 × 0.98-mm pixel size). The first series of DCE-MR images comprised 21 consecutive scans at 1-s intervals (the acquisition time for each scan was 14 s). A total of 0.2 mL/kg gadolinium-diethylenetriamine penta-acetic acid (Gd-DTPA; Magnevist Syringe; Nihon Schering, Osaka, Japan) was administered intravenously 6 s before a second scan at approximately 2.0 mL/s by manual injection. The total scan time of this series was 315 s.

After the acquisition of the first series of DCE-MR images, contrast-enhanced T1WIs (CE-T1WIs) with fat suppression were acquired using the same parameters as the unenhanced T1WIs approximately 6 min after Gd-DTPA administration in the axial plane. Subsequently, two series of DCE-MRIs were acquired as delayed and super-delayed phases at approximately 600 and 900 s after Gd-DTPA administration. Two consecutive scans were applied for the series of DCE-MRIs in the delayed and super-delayed phases, resulting in a total scan time of 30 s. DCE-MRI analyses were performed using the region of interest (ROI) technique and a workstation (Siemens). As illustrated in Fig. 1, the ROI was placed within the inner part of the cyst cavity except for the outer rim, which showed marked enhancement of the blood-pooling area (a). For the blood-flow area, the ROI was placed on the markedly enhanced area (b). The ROIs for the blood-pooling and blood-flow areas had an area of 130 and 37 mm^2, respectively.

The mean signal intensity (SI) of the ROI in each image was calculated and the TICs were constructed. The beginning of the first scan of the first series of DCE-MR images was designated as time 0.

On MR image slices distinct from previously reported slices [9], T1WIs showed a heterogeneous, low-to-intermediate SI (Fig. 2a). On T2WI, the lesion comprised two areas that demonstrated low SI and high SI (Fig. 2b). CE-T1WI acquired approximately 6 min after the administration of Gd-DTPA showed a heterogeneous SI, but whether the lesion was enhanced was unclear (Fig. 2c).

On DCE-MRI, the lesion was divided into two parts by reexamination according to the enhancement pattern: the blood-pooling and blood-flow areas. On T2WI, the blood-pooling area corresponded approximately to a high SI area and the blood-flow area corresponded approximately to a low SI area. The series of DCE-MRI of the blood-pooling area showed marked enhancement of the margin, but no enhancement in the inner part of the cavity (Fig. 3) and the TIC revealed no change in the SI until approximately 15 min after Gd-DTPA administration (Fig. 5a). The series of DCE-MR images of the blood-flow area showed marked enhancement in the cyst cavity in the early phase (Fig. 4). Additionally, the TIC revealed a rapid increase in the SI in the early phase, followed by a rapid decrease until 150 s, and then a gradual decrease until approximately 15 min after Gd-DTPA administration (Fig. 5b). The peak times of the blood-flow area, internal carotid artery, and jugular vein were 45, 30, and 45 s, respectively. The peak SIs of the blood-flow area, internal carotid artery, and jugular vein were 185, 303, and 201, respectively.

For histopathological evaluation, an incisional biopsy was performed under local anesthesia. This biopsy revealed that the lesion was filled with blood and had no epithelial lining. DSA was performed to evaluate the blood flow of the lesion because the biopsy suggested a diagnosis of ABC. DSA revealed that the lesion was supplied by the left inferior alveolar artery. Tumor blush was relatively weak and no arteriovenous shunt was depicted (Fig. 6). On the basis of the DSA findings, simple curettage of the lesion was performed without preoperative embolization and the intraoperative blood loss was massive (1050 cc). The histopathological findings demonstrated that the lesion comprised cyst wall-like highly cellular fibrous tissue that surrounded clotting blood. In the fibrous tissue, hemosiderin deposits, numerous knubbed cementum-like materials, and trabeculae of woven bones were observed, while giant cells were not prominent (Fig. 7). Histopathologically, the lesion was consistent with a diagnosis of ABC, although it included atypical findings. The postoperative course was uneventful and no recurrence was observed after 10 years.

Discussion

ABCs are classified as pseudocysts because they exhibit no epithelial lining. Additionally, they should be differentiated from true cysts or other pseudocysts (i.e., simple bone cysts with a static bone cavity) because their treatment is different. Furthermore, ABCs pose a heavy bleeding risk in surgery; thus, preoperative evaluation of the intralesional blood flow is necessary. Intra-arterial DSA is widely used for evaluating blood flow, but the procedure harbors some risks. Al-Ameri et al. reviewed several literature sources concerning the risks of angiography and reported that permanent neurological complication rates of angiography ranged from 0.4 to 2.4% [10]. CT angiography (CTA) is also useful for the delineation of blood vessels and may be less invasive than catheter angiography [11, 12]. However, although CTA is less invasive, the use of iodinated contrast medium poses a risk of contrast-induced nephropathy (CIN) [13]. The risk of serious acute CIN after diagnostic angiography or interventional angiography is now controversial [14], but CIN is the third leading cause of all hospital-acquired renal insufficiency [15]. Conversely, the use of MRI with Gd-based contrast agents is thought to be a relatively safe method considering the complication rates of the other two methods.

Several reports have evaluated MRI findings for ABC in the jaws [5, 8, 16–18]. The MR features of ABCs generally exhibit homogeneous intermediate SI on T1WI and high SI on T2WI [8]. Although the noncontrast-enhanced MR features of our case were almost consistent with previous reports, diagnosing this case as ABC was difficult. Minami et al. reported that CE-T1WIs show cyst walls with enhancement in all cases,

but no enhancement in the inner part of the cyst cavity [19]. At our institute, CE-T1WIs are acquired with a frequency-selective fat suppression technique to improve detection of enhanced areas. Unfortunately, in the present case, the enhancing effect of the lesion was weak or equivocal because of inadequate fat suppression.

In our case, the lesion could be divided into two parts according to the enhancement pattern on DCE-MRI. The MRIs of the blood-flow area showed heterogeneous, low-to-intermediate SIs on T1WI and low SI on T2WI. In contrast, the blood-flow area exhibited strong enhancement on DCE-MRI in the early phase. The series of DCE-MR images of the blood-flow area of the lesion showed marked enhancement in the early phase in the cyst cavity. The TIC revealed a rapid increase in the SI in the early phase, followed by a rapid decrease until 150 s, and finally a gradual decrease until approximately 15 min after the administration of Gd-DTPA. The series of DCE-MR images of the blood-pooling area of the lesion demonstrated marked enhancement in the margin, but no enhancement in the inner part of the lesion. The TIC showed no change in the SI until approximately 15 min after the administration of Gd-DTPA.

In our case, although the enhancing effect was unclear on CE-T1WI, strong enhancement was observed on DCE-MR images in the early phase. At the time of CE-T1WI acquisition, most of the contrast agent was washed away; thus, the enhancing effect might have been very weak. In the present ABC case, a rapid increase and decrease on DCE-MR images resulted in an equivocal enhancing effect on CE-T1WI. According to a previous report, some simple bone cysts show very weak enhancement on CE-T1WI [20]. This finding was similar to the current ABC case, but the TICs of the

ABCs showed a gradual increase, not “rapid increase and decrease.” When the enhancing effect of the lesion is weak or equivocal on CE-T1WI, DCE-MRI over time must be observed.

DSA is considered the “gold standard” in the assessment of vascularity, but not all ABCs exhibit intralesional blood flow [21, 22]. MRI has disadvantages in angiography [12], including a long scan time, low spatial and time resolution, and poor patient tolerance; thus, it cannot replace DSA. However, DCE-MRI is a less invasive method considering the risks of DSA, and might be a prerequisite for DSA.

In conclusion, we reported a case of ABC of the mandible in a 39-year-old woman. Evaluation of intralesional blood flow is important for ABC because of the hemorrhagic risk in surgery. In our case, preoperative DCE-MRI clearly delineated the vessel-rich area within the lesion.

References

1. Barnes L, Evenson JW, Reichart P, Sidransky D, editors. World Health Organization classification of tumours. Pathology and genetics of head and neck tumours. Lyon: IARC Press; 2005.

2. Vergel De Dios AM, Bond JR, Shives TC, McLeod RA, Unni KK. Aneurysmal bone cyst. A clinicopathologic study of 238 cases. Cancer. 1992;69:2921–31.

3. Kransdorf MJ, Sweet DE. Aneurysmal bone cyst: concept, controversy, clinical presentation, and imaging. AJR Am J Roentgenol. 1995;164:573–80.

4. Kalantar Motamedi MH. Aneurysmal bone cysts of the jaws: clinicopathological features, radiographic evaluation and treatment analysis of 17 cases. J Craniomaxillofac Surg. 1998;26:56–62.

5. Revel MP, Vanel D, Sigal R, Luboinski B, Michel G, Legrand I, et al. Aneurysmal bone cysts of the jaws: CT and MR findings. J Comput Assist Tomogr. 1992;16:84–6.

6. Ueno S, Mushimoto K, Kurozumi T, Hirase T, Takasu J. Aneurysmal bone cyst of the mandible. J Oral Maxillofac Surg. 1982;40:680–3.

7. Motamedi MH, Stavropoulos MF. Large radiolucent lesion of the mandibular condyle. J Oral Maxillofac Surg. 1997;55:1300–4.

8. Asaumi J, Konouchi H, Hisatomi M, Matsuzaki H, Shigehara H, Honda Y, et al. MR features of aneurysmal bone cyst of the mandible and characteristics distinguishing it from other lesions. Eur J Radiol. 2003;45:108–12.

9. Wakasa T, Asaumi JI, Konouchi H, Honda Y, Kishi K. Aneurysmal bone cyst of the mandible: a report of 2 cases and a review of the literature. Jpn J Oral Diagn/Oral Med. 2002;15:352–8.

10. Al-Ameri H, Thomas ML, Yoon A, Mayeda GS, Burstein S, Kloner RA, et al. Complication rate of diagnostic carotid angiography performed by interventional cardiologists. Catheter Cardiovasc Interv. 2009;73:661–5.

11. Herzig R, Burval S, Krupka B, Vlachová I, Urbánek K, Mares J. Comparison of ultrasonography, CT angiography, and digital subtraction angiography in severe carotid stenoses. Eur J Neurol. 2004;11:774–81.

12. Franklin B, Gasco J, Uribe T, VonRitschl RH, Hauck E. Diagnostic accuracy and inter-rater reliability of 64-multislice 3D-CTA compared to intra-arterial DSA for intracranial aneurysms. J Clin Neurosci. 2010;17:579–83.

13. Walsh SR, Tang T, Gaunt ME, Boyle JR. Contrast-induced nephropathy. J Endovasc Ther. 2007;14:92–100.

14. Acosta S, Björnsson S, Ekberg O, Resch T. CT angiography followed by endovascular intervention for acute superior mesenteric artery occlusion does not increase risk of contrast-induced renal failure. Eur J Vasc Endovasc Surg. 2010;39:726–30.

15. Nash K, Hafeez A, Hou S. Hospital-acquired renal insufficiency. Am J Kidney Dis. 2002;39:930–6.

16. Gadre KS, Zubairy RA. Aneurysmal bone cyst of the mandibular condyle: report of a case. J Oral Maxillofac Surg. 2000;58:439–43.

17. Hernandez GA, Castro A, Castro G, Amador E. Aneurysmal bone cyst versus hemangioma of the mandible. Report of a long-term follow-up of a self-limiting case. Oral Surg Oral Med Oral Pathol. 1993;76:790–6.

18. Matsuura S, Tahara T, Ro T, Masumi T, Kasuya H, Yokota T. Aneurysmal bone cyst of the coronoid process of the mandible. Dentomaxillofac Radiol. 1999;28:324–6.

19. Minami M, Kaneda T, Ozawa K, Yamamoto H, Itai Y, Ozawa M, et al. Cystic lesions of the maxillomandibular region: MR imaging distinction of odontogenic keratocysts and ameloblastomas from other cysts. AJR Am J Roentgenol. 1996;166:943–9.

20. Yanagi Y, Asaumi J, Unetsubo T, Ashida M, Takenobu T, Hisatomi M, et al. Usefulness of MRI and dynamic contrast-enhanced MRI for differential diagnosis of simple bone cysts from true cysts in the jaw. Oral Surg Oral Med Oral Pathol Oral Radiol Endod. 2010;110:364–9.

21. Bozbuğa M, Turan Süslü H. Aneurysmal bone cyst of the sphenoid bone extending into the ethmoid sinus, nasal cavity and orbita in a child. Turk Neurosurg. 2009;19:172–6.

22. Kumar VV, Malik NA, Kumar DB. Treatment of large recurrent aneurysmal bone cysts of mandible: transosseous intralesional embolization as an adjunct to resection. Int J Oral Maxillofac Surg. 2009;38:671–6.

Figure legends

Fig. 1.

The region of interest (ROI) setting for the blood-pooling and blood-flow areas (both images represent 45 s after the administration of gadolinium-diethylenetriamine penta-acetic acid (Gd-DTPA)).

For the blood-pooling area, the ROI was placed within the inner part of the cyst cavity except for the outer rim, which showed marked enhancement (a). For the blood-flow area, the ROI was placed on the markedly enhanced area (b). The ROIs for the blood-pooling and blood-flow areas had areas of 130 and 37 mm^2, respectively.

Fig. 2.

Magnetic resonance (MR) features of the lesion.

MR images revealed heterogeneous, low-to-intermediate signal intensities (SIs) on T1WI (a). On T2WI (b), a low SI area and a markedly high SI area were delineated. The contrast-enhanced T1WI images acquired approximately 6 min after administration of Gd-DTPA showed a heterogeneous SI, but the enhancement effect was unclear (c).

Fig. 3.

Series of dynamic contrast-enhanced (DCE)-magnetic resonance (MR) images of the blood-pooling area (selected images).

The series of DCE-MR images of the blood-pooling area demonstrated marked enhancement in the margin, but no enhancement in the inner part of the aneurysmal bone cyst.

Fig. 4.

The series of dynamic contrast-enhanced (DCE)-magnetic resonance (MR) images of the blood-flow area (selected images).

The series of DCE-MR images of the blood-flow area of the aneurysmal bone cyst (ABC) showed marked enhancement in the cyst cavity of the ABC.

Fig. 5.

The time-signal intensity curves (TICs) of the blood-pooling and blood-flow areas.

The TICs of the blood-pooling area exhibited no change in signal intensity (SI) until approximately 15 min after Gd-DTPA administration of (a). The TICs of the blood-flow area showed a rapid increase in SI in the early phase, followed by a rapid decrease until 150 s, and then a gradual decrease until approximately 15 min after Gd-DTPA administration (b).

Fig. 6.

Findings of digital subtraction angiography.

The lesion was supplied by the left inferior alveolar artery (arrow). Tumor blush was relatively weak (arrow head) and no arteriovenous shunt was depicted.

Fig. 7.

Photomicrograph of a specimen (hematoxylin and eosin staining; original magnification, ×200)

The lesion consisted of cyst wall-like, highly cellular fibrous tissue, surrounding clotting blood. In the fibrous tissue, hemosiderin deposits, numerous knobbed cementum-like material, and trabeculae of woven bones were observed, while giant cells were not prominent.

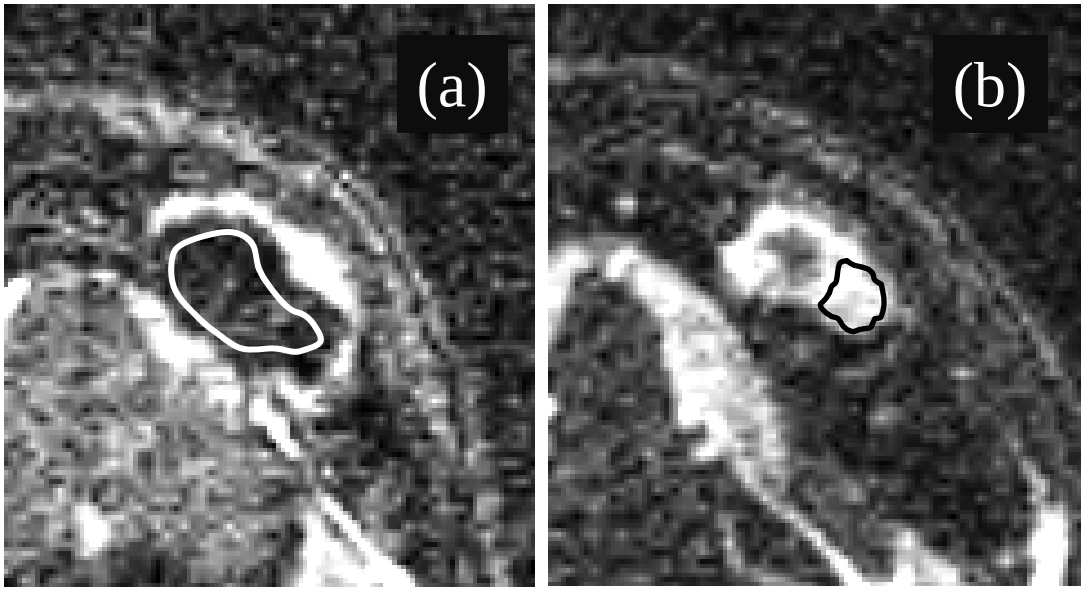

Fig. 1. ROI setting for the blood-pooling area and the blood-flow area (both images are at the time of 45 seconds after the administration of Gd.-DTPA). For the blood-pooling area, the ROI was placed within the inner part of the cyst cavity with the exception of the outer rim, which showed marked enhancement (a). For the blood-flow area, the ROI was placed on marked enhanced area (b). These ROIs had an area of 130 square millimeters and 37 square millimeters, respectively.

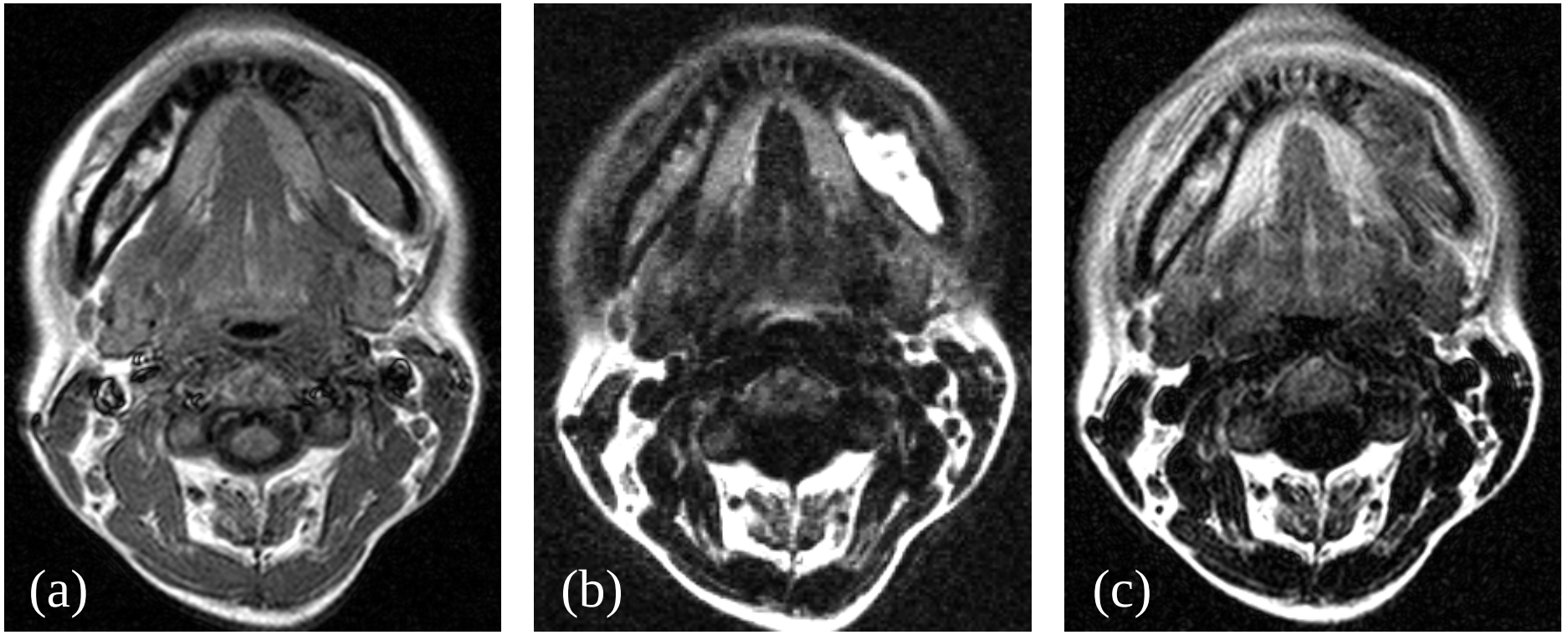

Fig. 2. MR features of the lesion.
The MRIs showed heterogeneous, low-to-intermediate SIs on T1WI (a). On T2WI (b), low SI area and marked high SI area were delineated. The contrast-enhanced T1WI acquired approx. 6 min after the administration of Gd.-DTPA showed heterogeneous SI, but enhancement-effect was unclear (c).

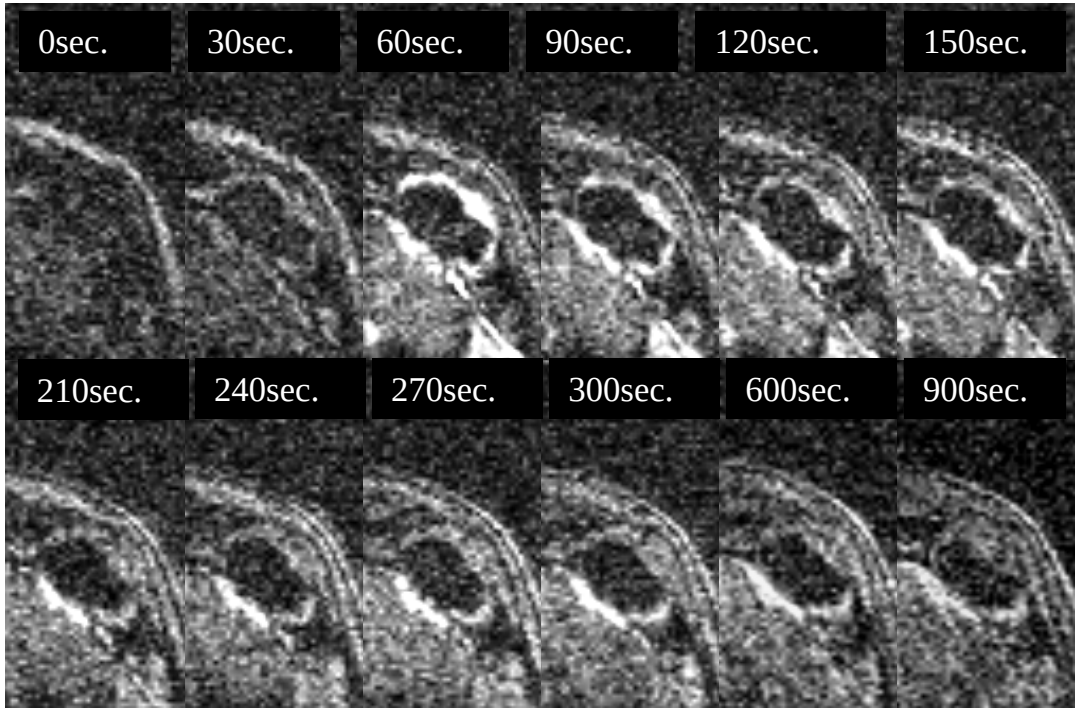

Fig. 3. The series of DCE-MRIs of the blood-pooling area (selected images from whole data).
The series of dynamic MRIs of the blood-pooling area shows marked enhancement in the margin, but no enhancement in the inner part of the ABC.

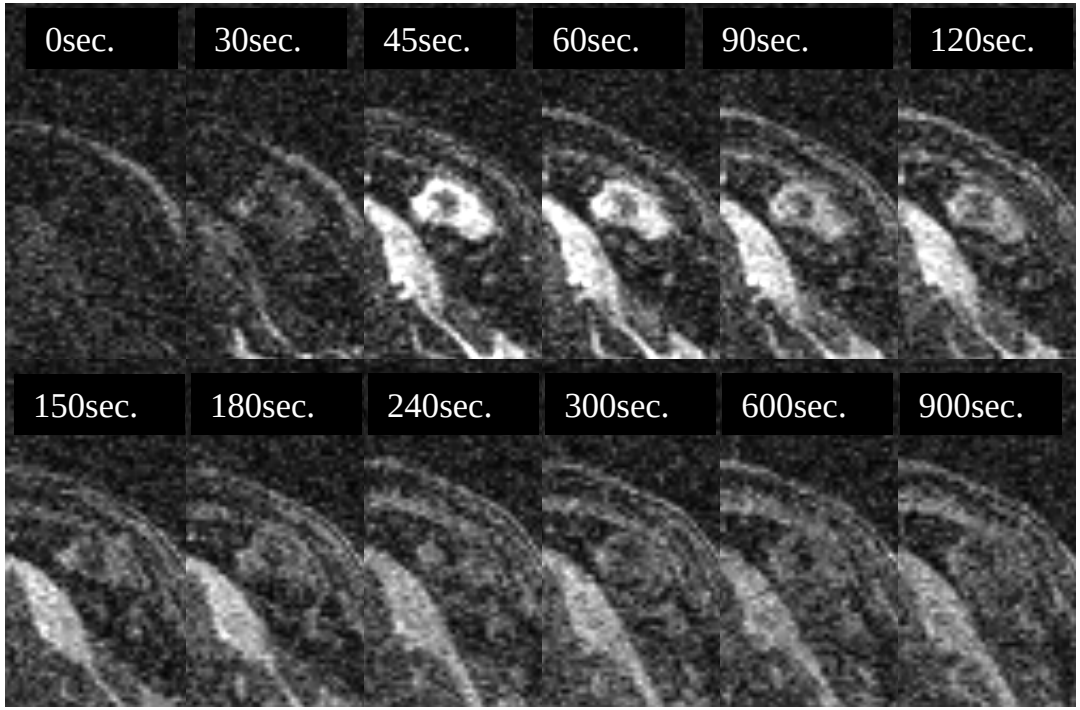

Fig. 4. The series of DCE-MRIs of the blood-flow area (selected images from whole data).
The series of dynamic MRIs of the blood-flow area of the ABC shows marked enhancement in the cyst cavity of the ABC.

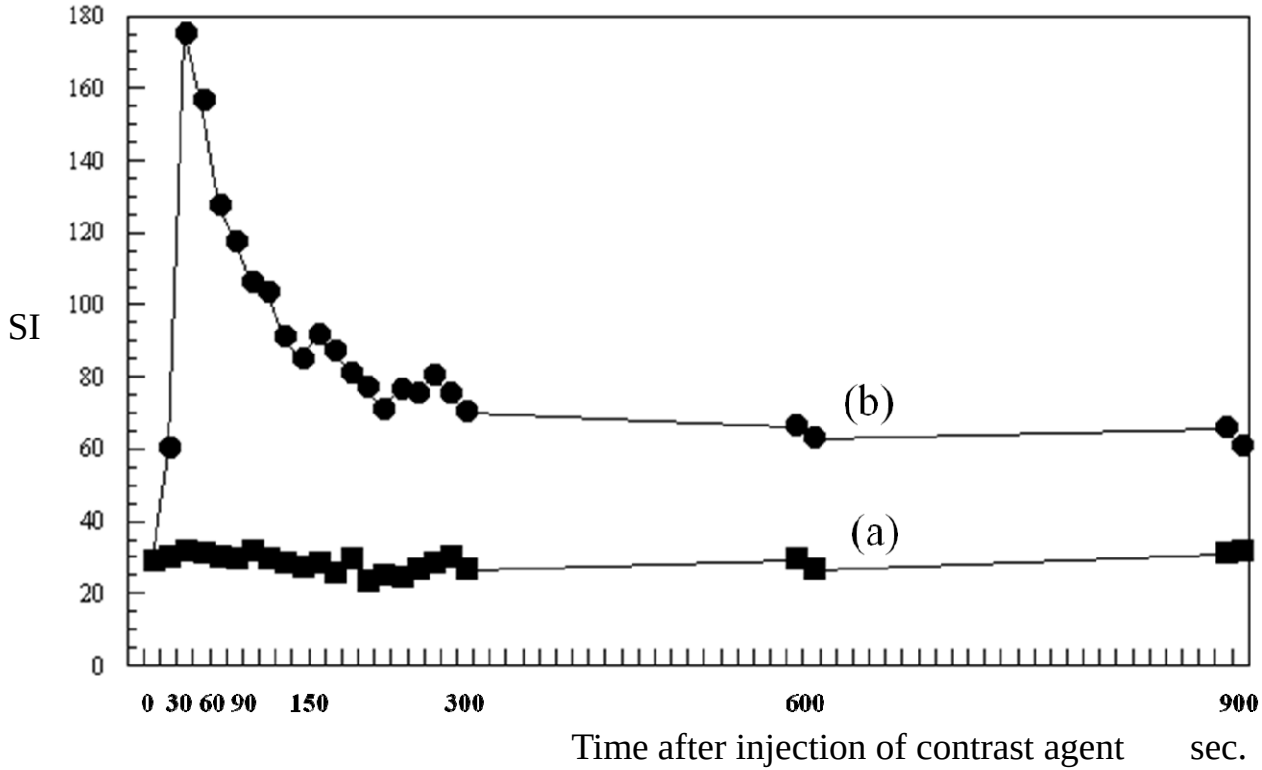

Fig. 5. The time-signal intensity curves of the blood-pooling area and the blood-flow area.

The time-signal intensity curves of the blood-pooling area show no change in the SI until approx. 15 min after the administration of Gd.-DTPA (a). The time-signal intensity curves of the blood-flow area show a rapid increase in the SI in the early phase, then a rapid decrease until 150 sec and a gradual decrease until approx. 15 min after the administration of Gd.-DTPA (b).

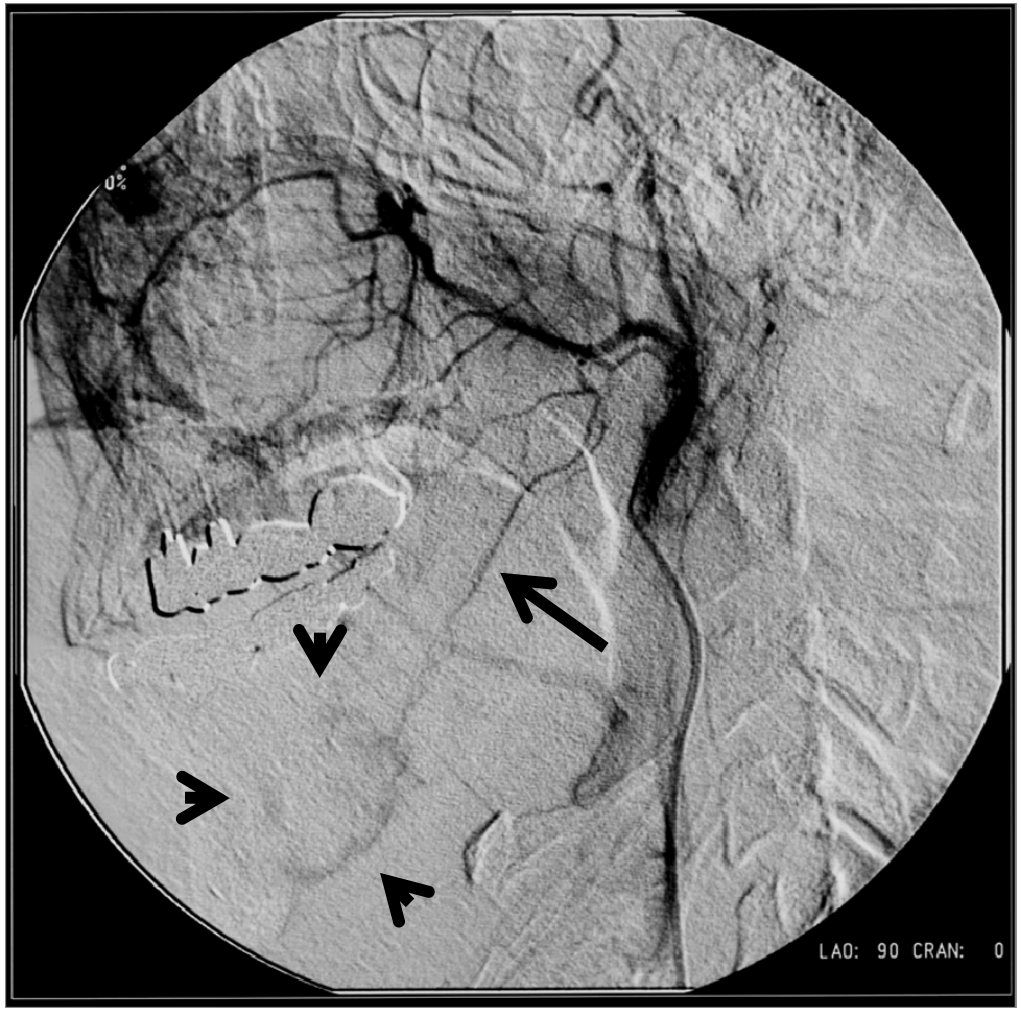

Fig. 6. The findings of digital subtraction angiography.
The lesion was supplied by left inferior alveolar artery(arrow). Tumor blush was relatively weak(arrow head) and no arterio-venous shunt was depicted.

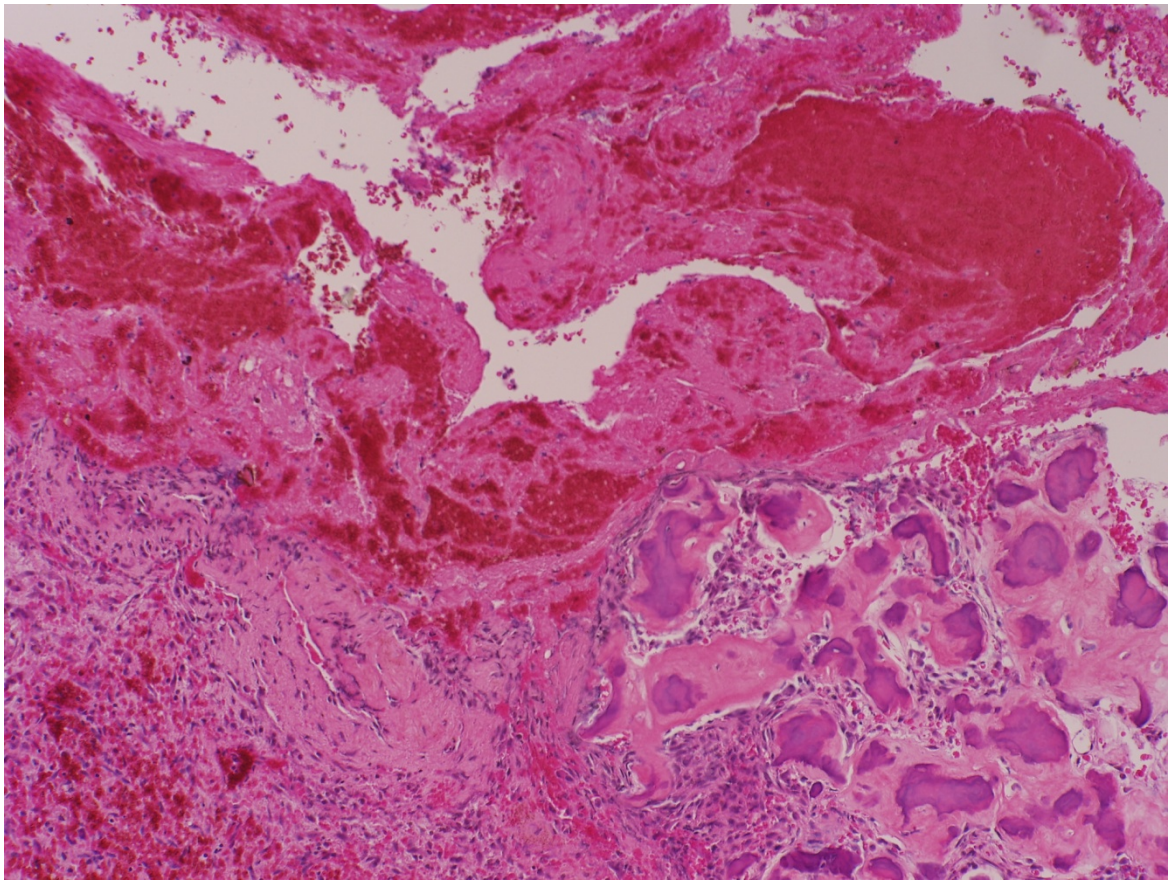

Fig. 7. Photomicrograph of a specimen (hematoxylin and eosin stains; original magnification ×200)
The lesion was composed of cyst wall like highly cellular fibrous tissue, which surrounds clotting blood. In the fibrous tissue, hemosiderin deposits, numerous knubbed cementum-like materials and trabeculae of woven bones, were observed, while giant cells were not prominent.